

Measurements of a rectangular confined jet

Chua L. P., Lua A. C. and Loh T. C. W.

School of Mechanical and Production Engineering

Nanyang Technological University, 50 Nanyang Avenue, Singapore 639798

Abstract

The paper presents the measurements of an air jet exiting from a rectangular nozzle of aspect ratio 6 into a confined chamber using an X-wire probe. Based on the mean velocity results, it was found that self-preservation had been achieved immediately after the potential core. Approximate self-preservation of the confined jet using turbulent intensities was established at $x/d=14$. The centreline velocity decay rate of the confined jet was found to be almost three times less than those of square and circular free jets but was about 28% greater than that of plane free jets with laminar initial conditions and similar Reynolds number. The spreading rate of the confined jet was found to be quite similar to those of the square and circular free jets but slightly less than the plane free jets.

Introduction

Fluidic flowmeters are flow measuring devices in which the operating principle is based on their intrinsic flow phenomenon, and have no mechanical moving parts. In these flowmeters, an oscillatory flow is formed whereby the frequency of the oscillations is directly proportional to the flow rate. In the target fluidic flowmeter which was first developed by Honda and Yamasaki [1], the incoming flow into the flowmeter first passes through a nozzle and then impinges upon a target in an enclosed chamber. The jet subsequently splits into two streams over the two sides of the target. For triggering the flow oscillations, there must be a flow imbalance in the two dividing streams. This necessitates lateral flow velocity fluctuations, and therefore the jet must be turbulent prior to its impact on the target. In a recent investigation [2], a new geometry of this target fluidic flowmeter makes use of the back wall to initiate and sustain flow oscillations thereby reducing the overall length as well as simplifying the design of the flowmeter. In an earlier study (Chua and Lua, [3]), the flow characteristics of the confined chamber with the same geometry as the fluidic flowmeter without target were investigated. However, as the measurements were carried out with just a single hot wire, there were other flow parameters that could not be studied. The objective of this paper was to study the flow characteristics of the fluidic flowmeter using the X-wire. It is hoped that with more flow parameters measured, the physics of the oscillating mechanism of the fluidic flowmeter can be better explained and subsequently its design improved.

Experimental arrangements

Atmospheric air was drawn into the confined test chamber ($24 \times 150 \times 500 \text{mm}^3$) as shown in Figure 1, through a 19mm internal diameter pipe by a three-phase oilless regenerative blower. The rectangular nozzle was located at the centre of the 500mm side of the confined chamber with a slot width d of 4mm and height 24mm. Measurements of mean and root-mean square (rms) velocities of the jet were carried out using X-wire probe, at Reynolds number ($=U_j d / \nu$, where U_j is the jet exit velocity and ν is the kinematic viscosity) of 5031, corresponding to $U_j = 20 \text{m/s}$. The X-wire ($\phi 5 \mu\text{m}$, Pt-10%Rh, Wollaston, length $\approx 1.0 \text{mm}$) were operated with the constant temperature anemometer made in-house, at an overheat ratio of 1.6. The included angle of the X-wire was about 90° and the

separation between the two wires was about 1.0mm. Due to space constraint of the confined jet, the calibration of the X-wire probe (including the calibration of the effective angle) was conducted away from the test chamber with a 25mm diameter nozzle. The X-wire probe was calibrated for velocity and yaw in the potential core of the circular jet, the range of yaw angles being -15° to 15° in 3° steps. Care had been taken to ensure that the orientation of the X-wire would not be disturbed when transferring the X-wire to the test section of confined jet for measurements. Signals from the X-wire were sent through a low pass filter of 1.6kHz. National Instrument data acquisition boards installed in an IBM PC were used to read instantaneous analog output signals with a sampling frequency of 3200 Hz and a total time of about 8 seconds for the 2 channels. The statistical parameters such as mean, root mean square and the cross correlation of the u and v were obtained using the program written in Matlab.

Results and discussion

The mean velocity distribution across the boundary layer at the nozzle exit follows the Blasius profile (not shown here). The normalizing length scale θ which is the boundary layer momentum thickness, equal to $0.019d$. At the centerline of the nozzle exit plane, the ratio U_{rms} / U_j was approximately 1.0%.

The U_{mean} velocity profiles in the range of $4 \leq x/d \leq 20$ are shown in Figure 2. U_0 was used as the normalizing scale for U_{mean} and the local lateral distance y was normalized by the local half width L . The profiles appear to collapse onto a single curve and self-preservation from $x/d = 5$ onwards were implied. Accuracy of this merge can be quite reliable; Tennekes and Lumley [4] had mentioned that measured mean velocity profiles in a plane jet appeared to be self-preserved beyond $x/d = 5$. The collapse of the profiles shows the establishment of self-preservation after the mixing layers merged on the jet axis, albeit Browne et al [5] had pointed out that the normalized mean velocity profiles for a wide range of flows were not sensitive indicators of self-preservation. Compared to the free jet as noted by Browne et al [5], the mean velocity profiles did not approach zero at higher y/L locations but staying at about 0.02 to 0.09 of U_0 . This may be due to the recirculation of the flow as elucidated by Chua and Lua [3].

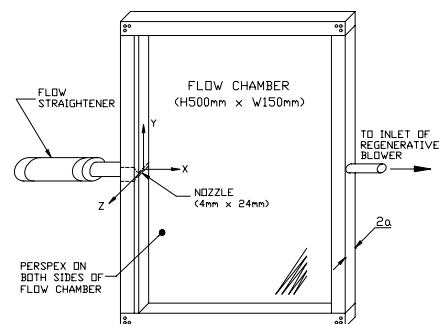


Figure 1 Schematic diagram of the confined jet

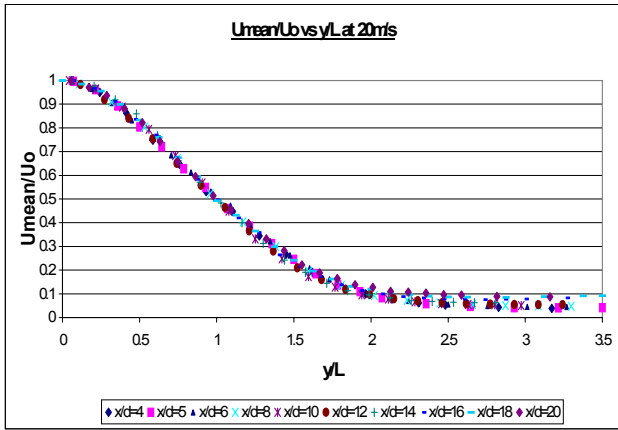


Figure 2 Distributions of U_{mean} at various streamwise stations.

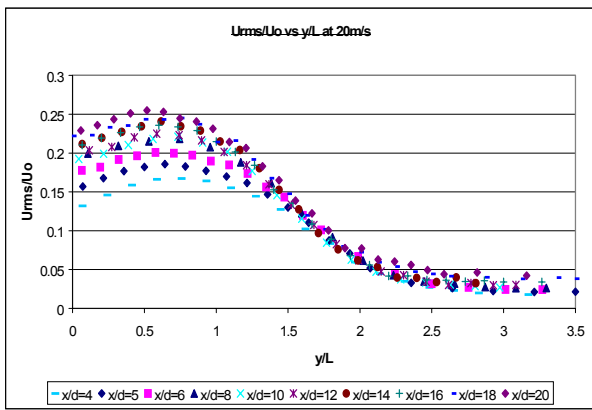


Figure 3 Distributions of U_{rms} at various streamwise stations.

Distributions of U_{rms} and V_{rms} using U_0 as normalizing scales are shown in Figures 3 and 4 respectively. Saddle-shaped distributions of the r.m.s. velocity profiles were observed in both Figures 3 and 4 and the profiles started to collapse at around $x/d = 14$. Appearance of convergence on the root mean square velocity profiles is a more reliable indication of self-preservation as suggested by Wynanski et al [6].

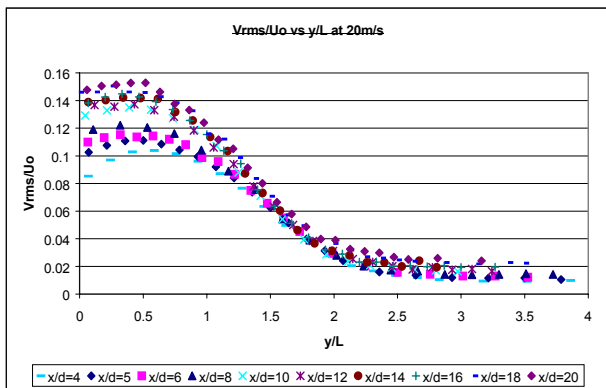


Figure 4 Distributions of V_{rms} at various streamwise stations

Distributions of uv_{mean} against y axis using U_0^2 and L as normalizing scales are shown in Figure 5. It could be seen that the velocity profiles become self-similar at $x/d = 16$. They also appeared to be flattened downstream tending towards zero. Convergence of the plot was a strong indication of self-preservation as claimed by Browne et al [5] and this showed the

reliability of self-preservation from the uv_{mean} graph. Since uv_{mean} values were derived from the essence and compilations of the u and v velocity fluctuating components, the non-exact zero of the graph at $y/L = 0$ was most probably attributed to experimental uncertainties.

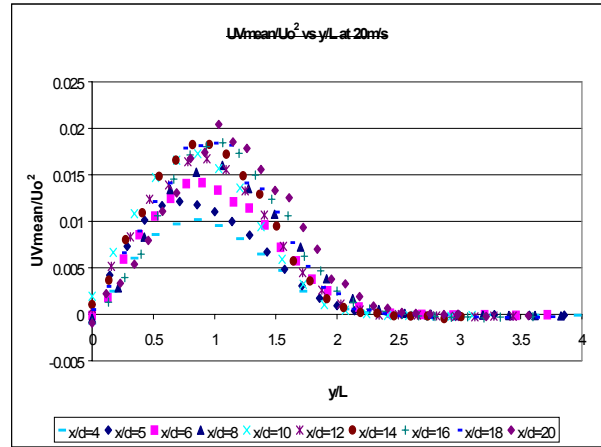


Figure 5 Distributions of normalized Reynolds shear stress at various streamwise locations.

Figure 6 shows the distributions of centreline r.m.s velocity, U'_{rms}/U_0 and V'_{rms}/U_0 along streamwise locations. In Figure 6, it could be observed that both U'_{rms}/U_0 and V'_{rms}/U_0 values became more stable as x/d values increased. This increment on U'_{rms}/U_0 and V'_{rms}/U_0 seemed to approach stability at $x/d = 18$. However, it would be too early to deduce that the centreline U_{rms} and V_{rms} have reached asymptote values due to the limited x/d values attainable in the present experimental arrangement.

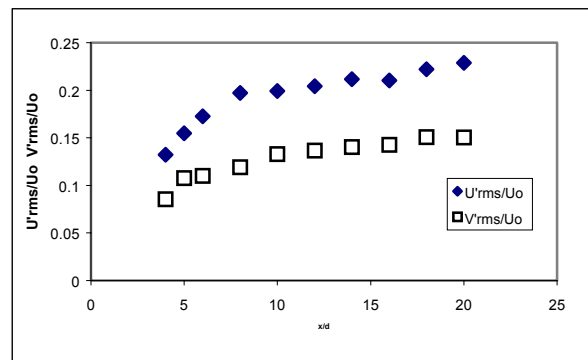


Figure 6 Distributions of the centerline root mean square axial and lateral velocity

Krothapalli et al[7] have shown that there are two regions of decay of U_0 for the rectangular free jet, namely, i) the two dimensional jet-type region that is $U_0 \sim x^{-1/2}$ extending from $4d$ to $60d$ and ii) the axisymmetric jet-type region that is $U_0 \sim x^{-1}$ extending beyond $60d$. It will be of interest to test the present U_0 with these two decay rates, to gain some insight, at least empirically, on the self-preservation state of U_0 .

For $U_0 \sim x^{-1/2}$ the normalized relationship can be expressed as

$$\left(\frac{U_j}{U_0}\right)^2 = K_d(x/d + C_k). \quad (1)$$

where K_d is the decay rate of the jet and C_k is the kinematic virtual origin of the jet. Figure 7 shows the variation of $(U_j/U_o)^2$ along different x/d locations. The values of $(U_j/U_o)^2$ appear to increase linearly with increasing x/d from $x/d=4.0$ onwards. Table 1 depicts a comparison of the present experiments with plane free jet types and shows that generally K_d values decrease with an increase in Reynolds number. The decay rate of the present jet is higher than that of Chua and Lua [3] with about the same Reynolds number.

For $U_o \sim x^{-1}$, the variations of mean centerline velocity U_o with x/d are plotted in Figure 8. The data within the range $4 \leq x/d \leq 20$ collapse reasonably well onto a straight line which can be expressed as

$$U_j/U_o = K_d(x/d + C_k) \tag{2}$$

Table 2 compares the K_d and C_k values obtained with those for square and circular free jets from other researchers. It could be observed from the table that decay rates for circular jets with laminar initial conditions were kept constant at about 0.18. The decay rates for the present confined rectangular jet were about two to three times less than those of free circular and square jets. However, these decay rates compare well with those of Chua and Lua [3].

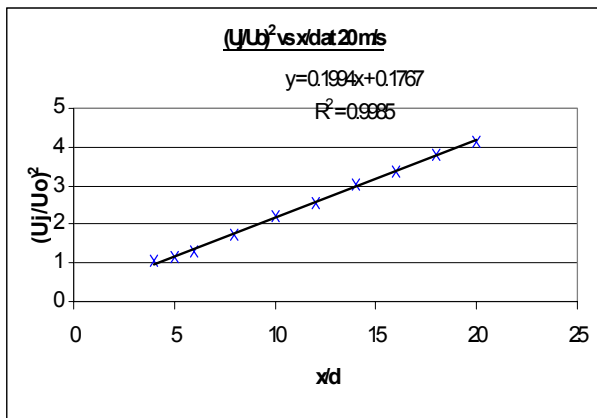


Figure 7 Variations of $(U_j/U_o)^2$ along the streamwise direction

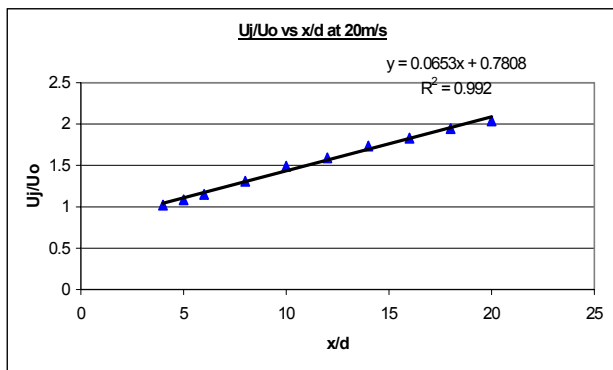


Figure 8 Variations of (U_j/U_o) along the streamwise direction

The K_d values in both equation (1) and (2) are higher than those obtained by [3], although the experiment was carried on the same test rig. This might be due to the constraints that the present measurements could not reach higher x/d locations due to the longer combination of X-wire probe and holder as compared with the single wire probe used in [3]. The range of

x/d used in the present curve fitting might not be long enough to reflect the effect of the U_o variation in the far field on the K_d obtained.

In Figure 9, the half widths (L) within the interaction region were plotted against their corresponding x/d . As with the decaying rate, a straight line was fitted into the plots to manifest their gradient and characteristic equation. The straight line can be expressed as

$$L/d = K_s (x/d + C_g) \tag{3}$$

where K_s is the spreading rate of the jet and C_g is the geometric virtual origin of the jet. The spreading rates of the different jet types approximated to about 0.1. A list of spreading rates is shown in Table 3

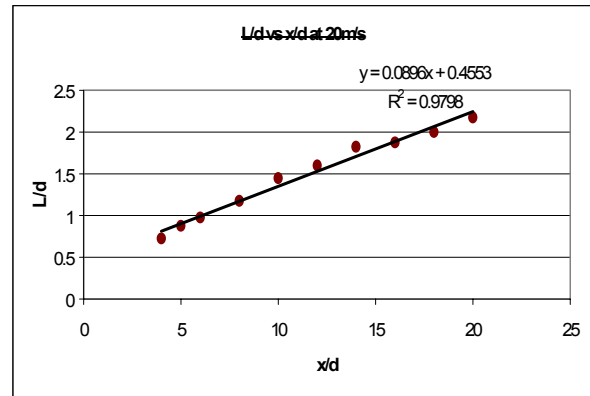


Figure 9 Streamwise variation of the half-width

Although Luafer [8] had mentioned that the spreading rates do not change with Reynolds number but would be affected by compressibility, a comparison in Table 3 would show that this might not be necessarily true. Some free jets spreading rates, such as those performed by Browne et al [5] and Hussain & Clark [9] were higher than those of confined jets, including the one in the present experiment. It could be postulated that Reynolds number, together with other necessary conditions such as centreline velocity decaying rate, jet initial conditions and compressing medium could well play a part in the spreading rate of the jet.

Conclusions

With initial laminar boundary conditions, the mean velocity, root mean square velocity and the Reynolds shear stress achieved self-preservation at distances of 5d, 14d and 16d respectively away from the jet exit. The centerline velocity decay rate of the confined jet was found to be almost three times less than those of square and circular free jets but was about 28% greater than that of plane free jets with laminar initial conditions and similar Reynolds number. It is deduced from the results obtained that although the confined jet is three-dimensional flow in nature, the decay rate of the confined jet follows more closely to that of a two-dimensional type of flow rather than that for a three-dimensional flow.

References

[1] Honda S. and Yamasaki H., Proc. of Int. Symp. on Fluid Contr. and Meas., Tokyo, 2, 623 (1985).
 [2] Lua A. C., Wee K. S., Chan W. K. and Liu C. Y., Proc. of Int. Symp. on Fluid Contr., Fluid Meas. and Visualization, Toulouse, France, 2, 899 (1994).
 [3] Chua L.P. and Lua A.C., Phys. Fluids, 10, 3137 (1988).
 [4] Tennekes H. and Lumley J.L., A first course in turbulence, USA Cambridge MIT Press, 1972.
 [5] Browne L.W.B., Antonia R.A. and Chambers A.J., J. Fluid Mech., 149, 355 (1984).

[6] Wagnanski I., Champagne F. and Marasli B., J. Fluid Mech., **168**, 31 (1986).
 [7] Krothapalli A., Baganoff D. and Karamcheti K., J. Fluid Mech., **107**, 210 (1978).
 [8] Laufer J., Transition & Turbulence, Acad. Press (1981).
 [9] Hussain F. and Clark A.R., Phys. Fluids, **20**, 1416 (1977).
 [10] Wagnanski I. and Fiedler H., J. Fluid Mech., **38**, 577 (1969).
 [11] Quinn W.R. and Militzer J., Phys. Fluids, **31**, 1017 (1988).

Investigator	Jet Type	Aspect Ratio	Reynolds No.	Initial Condition	K_d	C_k	Range
Browne et al [5]	Plane Free	19.69	7600	Laminar	0.143	9.0	$5 \leq x/d \leq 40$
Hussain & Clark [9]	Plane Free	44.03	32550	Laminar	0.1227	-4.47	$10 \leq x/d \leq 40$
Chua and Lua [3]	Rectangular	6.0	5517	Laminar	0.1564	0.5505	$6 \leq x/d \leq 30$
	Confined	6.0	2759	Laminar	0.1821	0.1432	$6 \leq x/d \leq 30$
Present	Rectangular Confined	6.0	5031	Laminar	0.1994	0.1767	$4 \leq x/d \leq 20$

Table 1 : Comparison of decay rates (K_d) and the virtual origins (C_k) for U_O ($\sim x^{-1/2}$)

Investigator	Jet Type	Aspect Ratio	Reynolds No.	Initial Condition	K_d	C_k	Range
Quinn & Militzer [11]	Round Free	NA	1.84×10^5	Unspecified	0.183	-0.33	$8.5 \leq x/d \leq 63$
	Square Free	1.0	1.84×10^5	Unspecified	0.185	-0.15	$8.4 \leq x/d \leq 62$
Wagnanski & Fiedler [10]	Round Free	NA	1×10^5	Unspecified	0.1724	-3.0	$10 \leq x/d \leq 50$
Chua and Lua [3]	Rectangular	6.0	5517	Laminar	0.0463	0.9623	$6 \leq x/d \leq 30$
	Confined	6.0	2759	Laminar	0.0512	0.8879	$6 \leq x/d \leq 30$
Present	Rectangular Confined	6.0	5031	Laminar	0.0653	0.7808	$4 \leq x/d \leq 20$

Table 2 : Comparison of decay rates (K_d) and the virtual origins (C_k) for U_O ($\sim x^{-1}$)

Investigator	Jet Type	Aspect Ratio	Reynolds No.	Initial Conditions	K_s	C_s	Range
Quinn & Militzer [11]	Square Free	1.0	184000	Unspecified	0.091	-1.02	$10 \leq x/d \leq 22$
	Round Free	N. A.	184000	Unspecified	0.087	0.65	$10 \leq x/d \leq 22$
Wagnanski & Fiedler [10]	Round Free	N. A.	100000	Unspecified	0.088	-	$10 \leq x/d \leq 90$
Browne et al [5]	Plane Free	19.69	7600	Laminar	0.104	5.00	$5 \leq x/d \leq 40$
Hussain & Clark[9]	Plane Free	44.03	32550	Laminar	0.1183	-2.150	$10 \leq x/d \leq 40$
Chua and Lua [3]	Rectangular	6.0	5517	Laminar	0.1029	0.1819	$6 \leq x/d \leq 30$
	Confined	6.0	2759	Laminar	0.0984	0.4234	$6 \leq x/d \leq 30$
Present	Rectangular Confined	6.0	5031	Laminar	0.0896	0.4553	$4 \leq x/d \leq 20$

Table 3 : Comparison of spread rates (K_s) and the virtual origins (C_s)